

Freestanding $La_2CuO_4/La_{1.55}Sr_{0.45}CuO_4$ heterostructure membranes with high-T_c interface superconductivity

Xueshan Cao(曹雪珊), Chuanyu Shi(史传宇), Yanzhi Wang(王彦智), Meng Zhang(张蒙), Jirong Sun(孙继荣), and Yanwu Xie(谢燕武)

Citation: Chin. Phys. B, 2025, 34 (**10**): 107301. DOI: 10.1088/1674-1056/adf4a3
http://cpb.iphy.ac.cn; http://iopscience.iop.org/cpb

What follows is a list of articles you may be interested in

Improving the electrical performances of InSe transistors by interface engineering

Tianjun Cao(曹天俊), Song Hao(郝松), Chenchen Wu(吴晨晨), Chen Pan(潘晨), Yudi Dai(戴玉頓), Bin Cheng(程斌), Shi-Jun Liang(梁世军), and Feng Miao(缪峰)

Chin. Phys. B, 2024, 33 (**4**): 047302. DOI: 10.1088/1674-1056/ad24d7

Comparison of resonant tunneling diodes grown on freestanding GaN substrates and sapphire substrates by plasma-assisted molecular-beam epitaxy

Xiang-Peng Zhou(周祥鹏), Hai-Bing Qiu(邱海兵), Wen-Xian Yang(杨文献), Shu-Long Lu(陆书龙), Xue Zhang(张雪), Shan Jin(金山), Xue-Fei Li(李雪飞), Li-Feng Bian(边历峰), and Hua Qin(秦华)

Chin. Phys. B, 2021, 30 (**12**): 127301. DOI: 10.1088/1674-1056/ac0525

Electrochemical liftoff of freestanding GaN by a thick highly conductive sacrificial layer grown by HVPE

Xiao Wang(王骁), Yu-Min Zhang(张育民), Yu Xu(徐俞), Zhi-Wei Si(司志伟), Ke Xu(徐科), Jian-Feng Wang(王建峰), and Bing Cao(曹冰)

Chin. Phys. B, 2021, 30 (**6**): 067306. DOI: 10.1088/1674-1056/abd6fa

Flattening is flattering: The revolutionizing 2D electronic systems

Baojuan Dong(董宝娟), Teng Yang(杨腾), Zheng Han(韩拯)

Chin. Phys. B, 2020, 29 (**9**): 097307. DOI: 10.1088/1674-1056/aba605

Electronic properties of the SnSe-metal contacts: First-principles study

Dai Xian-Qi (戴宪起), Wang Xiao-Long (王小龙), Li Wei (李伟), Wang Tian-Xing (王天兴)

Chin. Phys. B, 2015, 24 (**11**): 117308. DOI: 10.1088/1674-1056/24/11/117308

RAPID COMMUNICATION

Freestanding $La_2CuO_4/La_{1.55}Sr_{0.45}CuO_4$ heterostructure membranes with high-T_C interface superconductivity

Xueshan Cao(曹雪珊)[1], Chuanyu Shi(史传宇)[1], Yanzhi Wang(王彦智)[1], Meng Zhang(张蒙)[1], Jirong Sun(孙继荣)[1,2], and Yanwu Xie(谢燕武)[1,3,†]

[1] *School of Physics, Zhejiang University, Hangzhou* 310027, *China*
[2] *Beijing National Laboratory for Condensed Matter Physics & Institute of Physics, Chinese Academy of Sciences, Beijing* 100190, *China*
[3] *Collaborative Innovation Center of Advanced Microstructures, Nanjing University, Nanjing* 210093, *China*

(Received 29 April 2025; revised manuscript received 25 June 2025; accepted manuscript online 28 July 2025)

We report the fabrication of freestanding $La_2CuO_4/La_{1.55}Sr_{0.45}CuO_4$ (LCO/LSCO) heterostructure membranes, which were fabricated by selectively etching water-soluble $Sr_3Al_2O_6$ sacrificial layers from pulsed-laser-deposited heterostructures on $SrTiO_3$ substrates. Transport measurements reveal that these membranes exhibit superconducting behavior with an onset temperature of approximately 19 K. Comprehensive structural characterization using x-ray diffraction and scanning transmission electron microscopy demonstrates that the membranes retain excellent crystalline quality after release. The superconducting properties remain stable following mild post-annealing treatment under vacuum. This work establishes LCO/LSCO as a promising platform for developing flexible high-temperature superconducting interfaces, opening new possibilities for the development of flexible devices.

Keywords: freestanding, interfaces, superconductivity

PACS: 73.40.–c, 74.72.–h, 81.15.–z, 74.25.F–

DOI: 10.1088/1674-1056/adf4a3 **CSTR:** 32038.14.CPB.adf4a3

1. Introduction

Complex oxide interfaces provide a rich platform for exploring new quantum states and developing next-generation devices. When distinct perovskite oxides are combined, their interfaces frequently exhibit emergent phenomena absent from their constituent materials, most notably two-dimensional superconductivity. This has been clearly demonstrated in systems such as $LaAlO_3/SrTiO_3$ (LAO/STO),[1] FeSe/STO,[2] $La_2CuO_4/La_{2-x}Sr_xCuO_4$ (LCO/LSCO(x)),[3–5] and more recently in EuO/$KTaO_3$ and LAO/$KTaO_3$.[6–8] Among these, the LCO/LSCO(x) interface holds special significance because Sr-doped La_2CuO_4 is a prototypical high-temperature superconductor. Previous studies of substrate-supported LCO/LSCO(x) bilayers have revealed interfacial superconductivity with transition temperatures (T_C) above 30 K.[3–5] However, the fundamental question of whether such interfacial superconductivity can persist in freestanding membranes remains unexplored, representing a critical gap given the growing importance of freestanding oxides for both fundamental studies and applications in flexible electronics.[9,10]

Recent advances in thin-film exfoliation techniques have revolutionized the creation of freestanding complex oxide membranes.[11–15] $Sr_3Al_2O_6$ (SAO)[16] and $Sr_4Al_2O_7$,[17] which have been used as epitaxial sacrificial layers for synthesizing such membranes, provide a promising pathway. This has enabled the successful isolation of various functional oxides including STO,[16,18,19] $La_{0.7}Sr_{0.3}MnO_3$,[16] $BaTiO_3$,[20] $BiFeO_3$,[21] and even the high-T_C superconductor $YBa_2Cu_3O_{7-\delta}$ (YBCO),[22] with the resulting membranes largely retaining their bulk-like properties.

In this work, we prepared freestanding $La_2CuO_4/La_{1.55}Sr_{0.45}CuO_4$ (LCO/LSCO) heterostructure membranes by employing a sacrificial-layer method. The membranes maintain excellent crystallinity and show metallic behavior from room temperature down to 19 K, below which they become superconducting. These results demonstrate that interfacial superconductivity can be preserved in freestanding cuprate membranes.

2. Experiment methods

LCO/LSCO heterostructure membranes presented here were grown on 0.5-mm-thick STO (001) substrates by pulsed laser deposition (PLD) using a KrF excimer laser with a wavelength of 248 nm. Before film growth, the substrate was pre-annealed for 20 min at 975 °C under an oxygen pressure of 7.5×10^{-5} Torr to achieve a step-and-terrace surface. Then a 24-nm-thick epitaxial layer of SAO was grown as a sacrificial layer, using a laser energy density of 1.2 J/cm^2 and a repetition rate of 1 Hz. The substrate temperature was set to 730 °C and the oxygen pressure was kept at 5×10^{-6} Torr during de-

†Corresponding author. E-mail: ywxie@zju.edu.cn

© 2025 Chinese Physical Society and IOP Publishing Ltd. All rights, including for text and data mining, AI training, and similar technologies, are reserved.

position. After that, a 50-unit-cell (uc) STO layer and a 2-uc $SrLaAlO_4$ (SLAO) layer were subsequently grown as buffer layers, with a laser fluence of 1.2 J/cm^2 and a repetition rate of 2 Hz. The corresponding substrate temperature was 800 °C, and the oxygen pressure was 5×10^{-6} Torr. Above the buffer layers, a 25-uc-thick LSCO and a 25-uc-thick LCO layer were epitaxially grown in sequence, with a laser fluence of 1.2 J/cm^2 and a laser repetition rate of 4 Hz. The substrate temperature was 730 °C and the O_3 (a mixture of $\sim$ 10% O_3 and $\sim$ 90% molecular oxygen) pressure was 2×10^{-2} Torr, with a flow rate of 3 sccm without pumping. To prevent the degradation of the LCO/LSCO bilayers, a 2-uc-thick SLAO capping layer was grown under the same conditions as those of the LCO/LSCO bilayers. After deposition, the sample was cooled from 730 °C to 400 °C at a rate of 100 °C/min, while the O_3 flow rate was increased from 3 sccm to 10 sccm. The sample was held at 400 °C for 15 min before being cooled to room temperature, with an O_3 flow rate of 10 sccm. O_3 was turned off at 55 °C.

We monitored the film growth process via oscillations of a specularly reflected high-energy electron diffraction (RHEED) spot when available (Figs. S1(a)–S1(f)). RHEED patterns are streak-like after the growth of the SAO and SLAO layers, and spotty streaks after the growth of STO. However, the final RHEED patterns are characterized by two-dimensional features upon completion of the film growth. The deposition rate was carefully calibrated using the technique of x-ray reflectivity. The layer thickness of the heterostructures was determined by the number of laser pulses. Among these, the growth rates of LSCO and LCO were $\sim$ 0.014 uc/laser pulse and $\sim$ 0.010 uc/laser pulse, respectively.

Once grown, the heterostructure membrane was immersed into a potassium hydroxide solution (pH = 12) for 30 min to dissolve the SAO layer. A schematic diagram of the processing steps to release the LCO/LSCO heterostructure is shown in Fig. 1(a). The remaining heterostructure was captured by a flat polydimethylsiloxane (PDMS) sheet, which was made by covering a clean silicon wafer with 0.1-mm-thick PDMS glue (as the mechanical support), and transferred to a SiO_2 substrate and then released by heating the PDMS to 50 °C. Figure 1(b) is an optical image of the LCO/LSCO heterostructure on SiO_2. To test its robustness, the freestanding membrane was annealed again at 400 °C for 15 min under an O_3 atmosphere (O_3 flow rate = 10 sccm) and at 150 °C for 15 min under vacuum (background pressure 1×10^{-7} mbar), respectively.

3. Results

3.1. Structural characterizations

Atomic force microscopy (AFM) was employed to characterize the surface flatness of the sample. After the growth of the SAO and STO layers, the surface remains atomically flat, exhibiting well-defined steps and terraces (Fig. 1(c)). The root-mean-square roughness is as low as $\sim$ 0.34 nm, which provides an ideal template for subsequent film growth. In contrast, the surface of the fully grown heterostructure becomes slightly rougher, with a root-mean-square roughness of $\sim$ 1.50 nm (Fig. 1(d)).

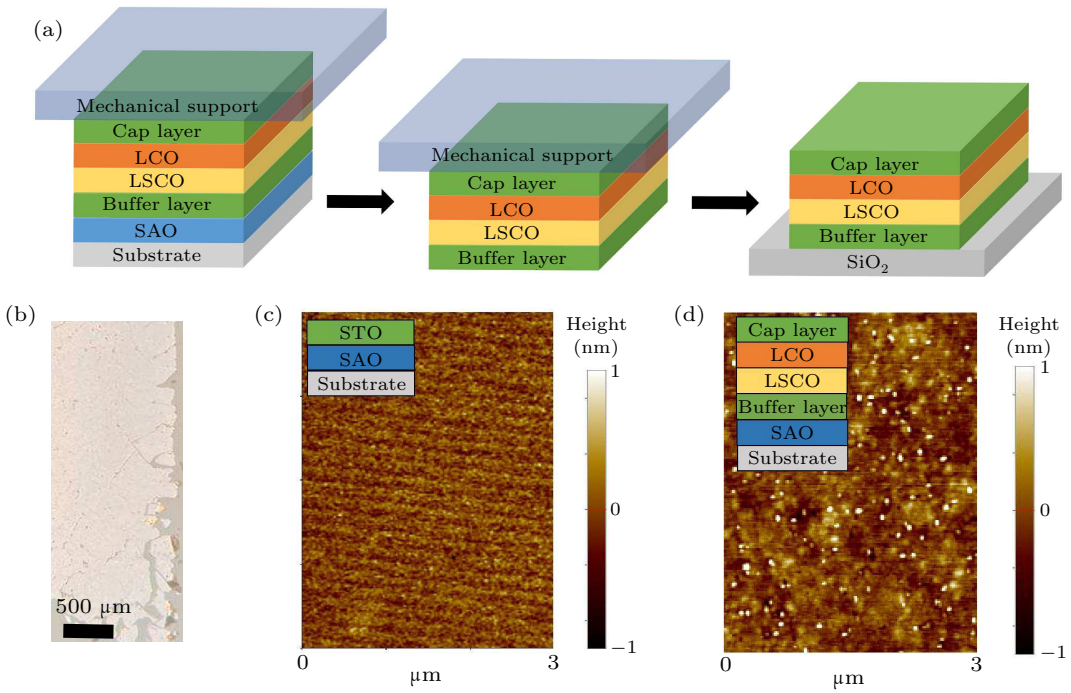


Fig. 1. (a) Schematic illustration of the processing steps used to transfer and release the LCO/LSCO heterostructure. (b) Optical image of the freestanding STO and SLAO-encapsulated LCO/LSCO heterostructure on SiO_2. (c), (d) Atomic force microscopy images of the STO layer surface (c) and the completed heterostructure (d). The scan areas are 3 μm × 4 μm, and the color scale ranges from −1 nm to 1 nm for both (c) and (d).

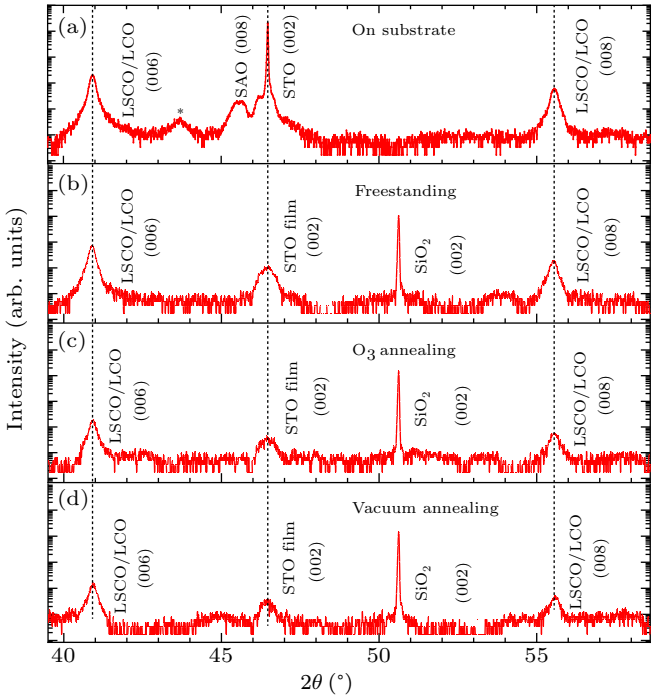


Fig. 2. XRD θ–2θ spectra of the LCO/LSCO heterostructure before (a) and after (b) release. (c), (d) XRD θ–2θ spectra of the freestanding LCO/LSCO heterostructure after O_3 annealing (c) and vacuum annealing (d). Dashed lines indicate the XRD peaks of the LCO/LSCO heterostructure and the STO film or substrate. The "*" symbol marks an artifact peak.

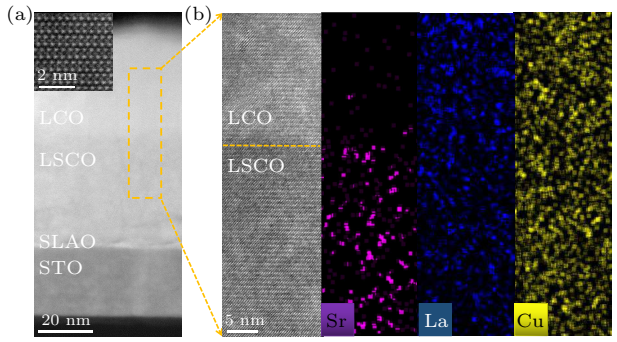


Fig. 3. (a) HAADF image of the cross section of the freestanding LCO/LSCO heterostructure, including the buffer and capping layers. The inset shows a close-up view of the LCO layer. (b) Left column: close-up of the LCO/LSCO interface; right three columns: elemental mappings. The dashed line indicates the position of the LCO/LSCO interface. All HAADF images were recorded along the [010] zone axis.

Figures 2(a) and 2(b) show the x-ray diffraction (XRD) spectra of the sample (a wide-angle XRD scan of the freestanding membrane is provided in Fig. S2). In addition to the substrate peaks, the XRD reflections of SAO and LCO/LSCO are clearly observed in the as-grown sample, whereas only the LCO/LSCO peaks remain after release. The release process only slightly affects the crystal structure of the LCO/LSCO bilayers: the out-of-plane lattice constant is ~13.21 Å for the as-grown sample, which is consistent with previous reports,[3–5] and ~ 13.24 Å for the freestanding sample. Moreover, the lattice constant of the freestanding LCO/LSCO membrane remains unchanged after post-annealing (400 °C for 15 min in O_3, Fig. 2(c); 150 °C for 15 min in vacuum, Fig. 2(d)), demonstrating the structural stability of the LCO/LSCO membrane. Notably, the XRD spectra of the as-grown sample exhibit a peak around 44°, which disappears in the freestanding membrane. A similar feature was observed in another sample (Fig. S3). We attribute this peak to a possible artifact phase formed during the growth of the SAO sacrificial layer.[16,17] In contrast, the peak at ~ 54° observed in the freestanding sample is likely due to impurities introduced during the transfer process.

To further evaluate the interface quality, scanning transmission electron microscopy (STEM) was performed on a representative freestanding sample. The high-angle annular dark-field (HAADF) images (Figs. 3(a) and 3(b)) together with energy-dispersive x-ray spectroscopy (EDS) elemental mappings (Fig. 3(b)) reveal coherent growth across all layers, with no significant intermixing detected at the LCO/LSCO interface.

3.2. Electrical properties

We examined the electrical transport properties of the samples. Figures 4(a) and 4(b) show the temperature dependence of the normalized resistance $R(T)/R(300\ \mathrm{K})$ for the LCO/LSCO heterostructure before and after etching the sacrificial SAO layer (raw data in Fig. S4). To ensure reliable electrical contacts, 50-nm-thick Ag pads were deposited via mask evaporation prior to the measurements. An optical image of the measurement configuration for the freestanding LCO/LSCO membrane is shown in the inset of Fig. 4(b).

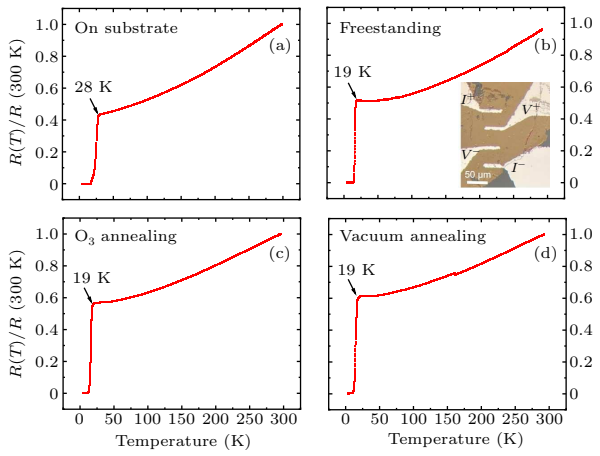


Fig. 4. Temperature-dependent normalized resistances of the as-grown LCO/LSCO heterostructure (a) and the freestanding LCO/LSCO heterostructure (b). Inset in (b): optical image showing the configuration for four-probe resistivity measurements of the freestanding sample. Temperature-dependent normalized resistances of the freestanding LCO/LSCO heterostructure after post-annealing in an O_3 atmosphere (c) or in vacuum (d).

Both the as-grown and the freestanding LCO/LSCO interfaces exhibit similar temperature-dependent behavior: the resistance decreases nearly linearly with decreasing temperature over a wide range from room temperature, and drops abruptly to zero upon entering the superconducting state.

The superconducting onset temperature (T_C^{onset}) is $\sim$ 28 K for the as-grown sample and $\sim$ 19 K for the freestanding sample (Figs. 4(a) and 4(b)). Despite the reduction after membrane release, the persistence of superconductivity demonstrates the robustness of the interfacial superconducting state in LCO/LSCO heterostructures. This reproducibility has been confirmed by measurements on multiple samples (Fig. S5). Furthermore, the T_C^{onset} of the freestanding membrane remains unchanged after post-annealing in different atmospheres (Figs. 4(c) and 4(d)). These results further highlight the stability of the superconducting state at the LCO/LSCO interface.

3.3. Discussion

The observed reduction in T_C^{onset} (from $\sim$ 28 K to $\sim$ 19 K) after membrane release may originate from two primary factors. First, surface adsorption of polar molecules on the freestanding membrane could perturb interfacial charge transfer between the LCO and LSCO layers — a critical requirement for establishing superconductivity in this system.[4,22–25] Control experiments revealed that uncapped membranes became fully insulating after exposure to potassium hydroxide solution, whereas a 2 uc SLAO capping layer effectively preserved superconductivity. Nevertheless, surface adsorbates still degrade transport, even in capped samples. This interpretation is supported by analogous observations in $LaAlO_3/SrTiO_3$ interfaces, where polar adsorbates substantially modified interfacial transport properties.[23,24]

Second, the *c*-axis lattice expansion observed after release (Fig. 2) may also contribute to the suppression of T_C. However, this appears contradictory to the conventional understanding that *c*-axis expansion typically enhances T_C in cuprates.[5,25–27] This apparent discrepancy underscores the need for further investigation to clarify the underlying mechanisms.

4. Summary

In summary, we have successfully fabricated freestanding crystalline LCO/LSCO heterostructure membranes that exhibit high-T_C interfacial superconductivity. The membranes were released through selective etching of a water-soluble SAO sacrificial layer in potassium hydroxide solution. Transport measurements reveal robust superconductivity in the freestanding membranes, with an onset transition temperature of $\sim$ 19 K. Notably, the superconducting properties remain stable after post-annealing treatments in different atmospheres, demonstrating both the structural and electronic integrity of the interface in the freestanding configuration.

Acknowledgments

We thank Sujuan Ding and Chuanhong Jin for assistance with STEM measurements. This work was supported by the National Natural Science Foundation of China (Grant Nos. 12325402 and 12074334) and the National Key R&D Program of China (Grant No. 2023YFA1406400).

References

[1] Reyren N, Thiel S, Caviglia A D, Kourkoutis L F, Hammerl G, Richter C, Schneider C W, Kopp T, Rüetschi A S, Jaccard D, Gabay M, Muller D A, Triscone J M and Mannhart J 2007 *Science* **317** 1196

[2] Ge J F, Liu Z L, Liu C, Gao C L, Qian D, Xue Q K, Liu Y and Jia J F 2015 *Nat. Mater.* **14** 285

[3] Gozar A, Logvenov G, Kourkoutis L F, Bollinger A T, Giannuzzi L A, Muller D A and Bozovic I 2008 *Nature* **455** 782

[4] Wu J, Pelleg O, Logvenov G, Bollinger A T, Sun Y J, Boebinger G S, Vanević M, Radović Z and Božović I 2013 *Nat. Mater.* **12** 877

[5] Den J, Ren T, Ju L, Zhang H, Sun J, Shen B and Xie Y 2020 *Sci. China Mater.* **63** 128

[6] Chen Z, Liu Z, Sun Y, Chen X, Liu Y, Zhang H, Li H, Zhang M, Hong S, Ren T, Zhang C, Tian H, Zhou Y, Sun J and Xie Y 2021 *Phys. Rev. Lett.* **126** 026802

[7] Liu C, Yan X, Jin D, Ma Y, Hsiao H W, Lin Y, Bretz-Sullivan T M, Zhou X, Pearson J, Fisher B, Jiang J S, Han W, Zuo J M, Wen J, Fong D D, Sun J, Zhou H and Bhattacharya A 2021 *Science* **371** 716

[8] Chen Z, Liu Y, Zhang H, Liu Z, Tian H, Sun Y, Zhang M, Zhou Y, Sun J and Xie Y 2021 *Science* **372** 721

[9] Ko H, Takei K, Kapadia R, Chuang S, Fang H, Leu P W, Ganapathi K, Plis E, Kim H S, Chen S Y, Madsen M, Ford A C, Chueh Y L, Krishna S, Salahuddin S and Javey A 2010 *Nature* **468** 286

[10] Nomura K, Ohta H, Takagi A, Kamiya T, Hirano M and Hosono H 2004 *Nature* **432** 488

[11] Novoselov K S, Geim A K, Morozov S V, Jiang D, Zhang Y, Dubonos S V, Grigorieva I V and Firsov A A 2004 *Science* **306** 666

[12] Dean C R, Wang L, Maher P, Forsythe C, Ghahari F, Gao Y, Katoch J, Ishigami M, Moon P, Koshino M, Taniguchi T, Watanabe K, Shepard K L, Hone J and Kim P 2013 *Nature* **497** 598

[13] Osada M and Sasaki T 2012 *Adv. Mater.* **24** 210

[14] Xu M, Liang T, Shi M and Chen H 2013 *Chem. Rev.* **113** 3766

[15] Butler S Z, Hollen S M, Cao L, *et al.* 2013 *ACS Nano* **7** 2898

[16] Lu D, Baek D J, Hong S S, Kourkoutis L F, Hikita Y and Hwang H Y 2016 *Nat. Mater.* **15** 1255

[17] Zhang J, Lin T, Wang A, Wang X, He Q, Ye H, Lu J, Wang Q, Liang Z, Jin F, Chen S, Fan M, Guo E J, Zhang Q, Gu L, Luo Z, Si L, Wu W and Wang L 2024 *Science* **383** 388

[18] Hong S S, Yu J H, Lu D, Marshall A F, Hikita Y, Cui Y and Hwang H Y 2017 *Sci. Adv.* **3** eaao5173

[19] Huang J K, Wan Y, Shi J, Zhang J, Wang Z, Wang W, Yang N, Liu Y, Lin C H, Guan X, Hu L, Yang Z L, Huang B C, Chiu Y P, Yang J, Tung V, Wang D, Kalantar-Zadeh K, Wu T, Zu X, Qiao L, Li L J and Li S 2022 *Nature* **605** 262

[20] Lu D, Crossley S, Xu R, Hikita Y and Hwang H Y 2019 *Nano Lett.* **19** 3999

[21] Peng B, Peng R C, Zhang Y Q, Dong G, Zhou Z, Zhou Y, Li T, Liu Z, Luo Z, Wang S, Xia Y, Qiu R, Cheng X, Xue F, Hu Z, Ren W, Ye Z G, Chen L Q, Shan Z, Min T and Liu M 2020 *Sci. Adv.* **6** eaba5847

[22] Chen Z, Wang B Y, Goodge B H, Lu D, Hong S S, Li D, Kourkoutis L F, Hikita Y and Hwang H Y 2019 *Phys. Rev. Mater.* **3** 060801(R)

[23] Zhang M, Chen Z, Mao B, Li Q, Bo H, Ren T, He P, Liu Z and Xie Y 2018 *Phys. Rev. Mater.* **2** 065002

[24] Chen Z, Chen X, Mao B, Li Q, Zhang M, Bo H, Liu Z, Tian H, Zhang Z and Xie Y 2018 *Adv. Mater. Interface* **5** 1801216

[25] Locquet J P, Perret J, Fompeyrine J, Mächler E, Seo J W and Van Tendeloo G 1998 *Nature* **394** 453

[26] Sato H, Tsukada A, Naito M and Matsuda A 2000 *Phys. Rev. B* **61** 12447

[27] Johnson M A, Burquest J F, Larsen M H and Prill N 2018 *Thin Solid Films* **649** 167